Published in final edited form as:
NMR Biomed. 2006 May ; 19(3): 352–361.

Phased array ghost elimination

Peter Kellman* and **Elliot R. McVeigh**
Laboratory of Cardiac Energetics, National Institutes of Health, National Heart, Lung and Blood Institute, Bethesda, MD 20892-1061, USA

Abstract

Parallel imaging may be applied to cancel ghosts caused by a variety of distortion mechanisms, including distortions such as off-resonance or local flow, which are space variant. Phased array combining coefficients may be calculated that null ghost artifacts at known locations based on a constrained optimization, which optimizes SNR subject to the nulling constraint. The resultant phased array ghost elimination (PAGE) technique is similar to the method known as sensitivity encoding (SENSE) used for accelerated imaging; however, in this formulation is applied to full field-of-view (FOV) images. The phased array method for ghost elimination may result in greater flexibility in designing acquisition strategies. For example, in multi-shot EPI applications ghosts are typically mitigated by the use of an interleaved phase encode acquisition order. An alternative strategy is to use a sequential, non-interleaved phase encode order and cancel the resultant ghosts using PAGE parallel imaging. Cancellation of ghosts by means of phased array processing makes sequential, non-interleaved phase encode acquisition order practical, and permits a reduction in repetition time, *TR*, by eliminating the need for echo-shifting. Sequential, non-interleaved phase encode order has benefits of reduced distortion due to off-resonance, in-plane flow and EPI delay misalignment. Furthermore, the use of EPI with PAGE has inherent fat-water separation and has been used to provide off-resonance correction using a technique referred to as lipid elimination with an echo-shifting N/2-ghost acquisition (LEENA), and may further generalized using the multi-point Dixon method. Other applications of PAGE include cancelling ghosts which arise due to amplitude or phase variation during the approach to steady state. Parallel imaging requires estimates of the complex coil sensitivities. *In vivo* estimates may be derived by temporally varying the phase encode ordering to obtain a full *k*-space dataset in a scheme similar to the autocalibrating TSENSE method. This scheme is a generalization of the UNFOLD method used for removing aliasing in undersampled acquisitions. The more general scheme may be used to modulate each EPI ghost image to a separate temporal frequency as described in this paper.

Keywords

PAGE, SENSE; TSENSE; ghost cancellation; phased array; parallel imaging; cardiac imaging; EPI

INTRODUCTION

Background

Phased array reconstruction (1), which employs coil sensitivity (B1) maps as weights for phased array combining, has been shown to optimize SNR, and, in addition, provide a degree of artifact suppression for alias ghosts. Phased array combining based on parallel imaging may be applied to cancel ghosts caused by a variety of distortion mechanisms, including distortions such as off-resonance or local flow, which are space variant. Phased array combining coefficients may be calculated that null ghost artifacts at known locations based on a

*Correspondence to: P. Kellman, Laboratory of Cardiac Energetics, National Institutes of Health, National Heart, Lung and Blood Institute, 10 Center Drive, MSC-1061, Bldg 10, RM B1D 416, Bethesda, MD 20892-1061, USA. E-mail: kellman@nih.gov

constrained optimization, which optimizes SNR subject to the nulling constraint. The resultant phased array ghost elimination (PAGE) technique (2) is similar to the method known as sensitivity encoding (SENSE) used for accelerated imaging; however, in this formulation it is applied to full field-of-view (FOV) images. The SENSE technique (3), which also performs phased array combining, is typically used to accelerate imaging by acquiring a reduced FOV in the phase encode direction. In this case, ghost images caused by the intentional aliased acquisition are then removed by phased array processing. We present a general formulation to eliminate ghosts, which applies 'SENSE' directly to the full *k*-space reconstruction.

In the PAGE method, 'SENSE' is applied directly to the full *k*-space reconstruction and ghost separated images are produced in which each image is weighted by the respective value of the ghost point spread function. These component ghost images may be combined either coherently, using a complex weighted sum, if the point spread function is known, or non-coherently, using the root-sum-of-squares method. PAGE may be alternatively implemented by applying the phased array combiner (SENSE reconstruction) after deinterleaving the raw *k*-space. Application of SENSE (4) and SMASH (5) to EPI ghost elimination was described in which odd and even lines were deinterleaved, processed separately and non-coherently combined. In this alternative implementation, multiple images produced from the deinterleaved *k*-space data are weighted by the Fourier coefficients of the ghost point spread function (PSF). Both methods for PAGE are described and compared. The primary difference other than computational aspects is the method of combining images following parallel imaging.

Phased array combining which optimizes SNR subject to nulling constrains is also known as the generalized sidelobe canceller (6). Adaptive phased array combining in an MRI context (7) has been formulated in which the complex weights are derived using sample correlation estimates, based on a stochastic signal model. This adaptive method has been further applied to ghost cancellation (7), by using sample 'noise' statistics measured near the source of the artifact, which serves to null the artifact as well as the region of the desired image that corresponds to the source of the artifact. However, in this method, the extent of the spatial null is fairly broad.

As in the conventional application of SENSE for partial FOV accelerated imaging, the phased array method for ghost cancellation incurs a similar loss in signal-to-noise ratio due to the ill-conditioning of the inverse solution. However, in this full FOV imaging application, there is no additional loss in SNR due to acceleration. While the theoretical formulation presented in this paper may be generalized to show that distortion with quite general point spread function may be eliminated by the phased array artifact cancellation method, the performance of phased array processing, which depends on the number of coils and sensitivity maps, poses practical limitations on which type of distortion may be cancelled effectively. Typical surface coils have relatively slow spatial variation. Therefore, de-blurring, in which case point spread values are closely spaced, is not practical since the inverse solution is correspondingly ill-conditioned. However, widely spaced ghost artifacts may be readily cancelled, as demonstrated experimentally.

EPI application

Echo-planar imaging (EPI) is widely used for ultra-fast imaging. A number of techniques (8-16) are used to minimize distortion and ghost artifacts, which result from phase and amplitude errors between echoes. The phased array processing method for ghost cancellation adds yet another tool which may be incorporated to further mitigate EPI distortion and artifacts. Application to multi-shot EPI with sequential, non-interleaved phase encode acquisition order is described. Cancellation of ghosts by means of phased array processing makes sequential, non-interleaved phase encode acquisition order practical, and has a number of benefits such as reduced distortion due to off-resonance, in-plane flow and EPI delay misalignment, as well

as eliminating the need for echo-shifting. Incorporating this phased array method for ghost cancellation may result in greater flexibility in designing acquisition strategies. Multi-shot EPI has been applied to cardiac imaging with SSFP for reduction of TR by eliminating echo time shifting (17). A degree of fat suppression is achieved by PAGE simply using the first signal component (assumed to be on resonance) and ignoring the other components (2,17). An estimate of the space variant 'point spread function' and/or separated images at individual echo times may be derived as a by-product of the reconstruction which may be used to perform off-resonance correction as described in the technique for fat-water separation referred to as lipid elimination with an echo-shifting N/2-ghost acquisition (LEENA) (18) or using the more general iterative least squares multi-point Dixon solution (19).

Parallel imaging requires estimates of the complex coil sensitivities. *In vivo* estimates may be derived by temporally varying the phase encode ordering to obtain a full *k*-space dataset in a scheme similar to the autocalibrating TSENSE method. This scheme is a generalization of the UNFOLD method (20) used for removing aliasing in undersampled acquisitions. The more general scheme may be used to modulate each EPI ghost image to a separate temporal frequency as described in this paper.

METHODS

Theory

Superimposed images (ghosts) may be separated by phased array combining with appropriate weights, calculated by the inverse solution formulated as follows. The reconstructed image with ghosts, $g_i(x,y,t)$, for the ith coil at time t may be written as:

$$g_I(x,\ y,\ t) = \sum_{k=0}^{N_g} s_i(x,\ y - kD)h_k(x,\ y - kD,\ t)\, f(x,\ y - kD,\ t) + n_I(x,\ y,\ t) \quad (1)$$

where $f(x,y,t)$ is the desired image, $s_i(x,y)$ is the complex field sensitivity for the ith coil, N_g is the number of ghosts (N_g + 1 superimposed images) with spacing D, $h_k(x,y,t)$ is the complex weight of the kth ghost arising from the signal at (x,y), $n_i(x,y,t)$ is the observation noise, and (x,y) variables are assumed to be discrete as a result of image reconstruction from a finite set of periodic k-space samples. As a result of periodic k-space sampling with spacing Δk_y between phase encode lines, $f(x,y)=f(x,y\text{-}FOV_y)$, where $FOV_y=1/\Delta k_y$ is the full field-of-view in the phase encode direction. Equation (1) may be used to model a wide range of ghost mechanisms which create a periodic variation in k-space weighting, such as EPI acquisition or transient approach to interrupted steady state (21). However, the practical ability to eliminate ghosts using the parallel imaging method is set by the number and spacing of ghosts and the coil sensitivity profiles which together determine the performance of the inverse solution. The image weight, h_k will be referred to as a 'point spread function' (PSF), even though it is understood that it is a function of (x,y) and, therefore, is actually space variant, due to spatial variation in tissue T_1, T_2, and off-resonance effects from chemical shift and field inhomogeneity. For reception with N_c coils, eqn (1) may be written in matrix form as

$$\begin{bmatrix} g_1(x,\ y) \\ \vdots \\ g_{N_c}(x,\ y) \end{bmatrix} = \begin{bmatrix} s_1(x,\ y) & \dots & s_1\left(x,\ y - N_g D\right) \\ \vdots & & \vdots \\ s_{N_c}(x,\ y) & \dots & s_{N_c}\left(x,\ y - N_g D\right) \end{bmatrix} \times \begin{bmatrix} h_0(x,\ y) f(x,\ y) \\ \vdots \\ h_{N_g}\left(x,\ y - N_g D\right) f\left(x,\ y - N_g D\right) \end{bmatrix} + \begin{bmatrix} n_1(x,\ y) \\ \vdots \\ n_{N_c}(x,\ y) \end{bmatrix} \tag{2}$$

or more compactly as

$$\mathbf{g}(x,\ y) = \mathbf{S}(x,\ y)\mathbf{v}(x,\ y) + \mathbf{n}(x,\ y) \tag{3}$$

where the matrix and vectors in eqn (3) are in direct correspondence with eqns (1) and (2), and the time index t is suppressed to simplify the equations. The elements of the vector $\mathbf{v}$ are the separated ghost images $h_k(x,y–kD)f(x,y–kD)$, which include the point spread weighting by h_k.

Equation (3) becomes over-determined (more equations than unknowns) when the number of coils, N_c, is greater than the number of superimposed signals, $N_g + 1$, and $\mathbf{v}(x,y)$ can be estimated in a least squares sense, given estimates for the complex coils sensitivities (B1 maps) $s_i(x,y)$, as well as knowledge of the number of ghosts N_g and spacing D. The weighted least squares estimate $\hat{\mathbf{v}}(x,y)$ of $\mathbf{v}$ (x,y), which optimizes SNR, may be written as

$$\begin{aligned} \hat{\mathbf{v}}(x,\ y) &= \left[\mathbf{S}(x,\ y)^{\mathrm{H}}\mathbf{R}_n^{-1}\mathbf{S}(x,\ y)\right]^{-1}\mathbf{S}(x,\ y)^{\mathrm{H}}\mathbf{R}_n^{-1}\mathbf{g}(x,\ y) \\ &= \mathbf{U}(x,\ y)\,\mathbf{g}(x,\ y) \end{aligned} \tag{4}$$

where $\mathbf{R}_n$ is the noise covariance matrix, the superscript $^{\mathrm{H}}$ denotes the conjugate transpose or Hermitian operator, and the ‘unmixing’ matrix $\mathbf{U}$ defined by this equation is $N_g + 1$ rows by N_c columns. The kth component of the vector $\hat{\mathbf{v}}(x,y)$ is an estimate of $h_k(x,y–kD)f(x,y–kD)$, a weighted and shifted version of the image $f(x,y)$. The individual component ghost images of $\hat{\mathbf{v}}(x,y)$ may be spatially aligned (shifted in y-direction) and combined to gain an improved estimate of the desired image $f(x,y)$. Hence, it is sufficient to know the ghost spacing and not necessary to know the space variant point spread function $h_k(x,y)$ in order to cancel the ghosts. It is important to recognize that while the ghosts may be separated, and therefore no longer interfere with each other, the individual ghost images are still weighted by their respective PSF values, $h_k(x,y)$. The separated ghost images may be combined to create a single image which is approximately proportional to the desired image $f(x,y)$ since in many cases the point spread function (h_k) has a nearly constant norm value (i.e. $\sqrt{[\Sigma_k|h_k(x,y)|^2]}$ is fairly independent of x,y). This is the case when the ghosts arise due to off-resonance phase accrual, for which the total energy of each pixel does not change as the distribution changes across the ghosts. Estimates of the complex PSF h_k may be used to optimize SNR when combining the individual separated ghost images (2).

A block diagram of the signal processing steps for artifact cancellation described above is shown in Fig. 1. Note that the $(N_g + 1) \times N_c$ unmixing matrix $\mathbf{U}$ may either be applied to the $N_c \times 1$ image vector $\mathbf{g}$ explicitly, as formulated, and then each component image of $\hat{\mathbf{v}}$ is (x,y) aligned, or alternatively, as shown in the implementation of Fig. 1, the shifting of components

can be performed prior to array combining. In this case, shown by re-writing eqn (1) for $g_i(x,y-kD)$, the array combiner weights (for all components) are simply the first row of the matrix **U**. The sample images illustrate the case of N_c=4 coils and N_g=1 ghost with D=FOV/2. The phased array combiner refers to the parallel imaging operation which is a weighted sum of individual coil images, whereas the image combiner step combines the separated ghost images following parallel imaging.

The individual component images, separated in this manner, are each weighted by complex PSF values $h_k(x,y,t)$, determined by the tissue parameters and off-resonance, as well as magnetization preparation. An alternative scheme based on deinterleaving the raw *k*-space data and applying SENSE image reconstruction is diagrammed in Fig. 2. In this implementation, the deinterleaving factor equals the number of superimposed images (N_g + 1) assumed to have periodic spacing across the FOV. The ghosts are caused by the periodic amplitude or phase distortion of the *k*-space data which may be represented by the complex *k*-space weights H_m, m=0, 1, … , N_g. In general the distortion mechanism is space variant and the *k*-space coefficients $H_m(x,y)$ depend on contributions of a pixel at (x,y), for example due to off-resonance or local flow. The corresponding values of the discrete point spread function $h_m(x,y)$ (space variant) are derived from the (N_g+1)-point discrete Fourier transform, i.e.

$$h_m(x,y) = \sum_{k=0}^{Ng} H_k(x,y) e^{-i2\pi km/(Ng+1)} \tag{5}$$

The schemes depicted by Figs. 1 and 2 are equivalent by proper choice of image combining following parallel imaging. The schemes may be made equivalent by incorporating a DFT into the complex image combiner. For example for N_g=1, this is simply the 2 point DFT, i.e. the sum and difference of images m=0 and m=1. However, in general, these two schemes will not be the same. For example, if root-sum-of-squares magnitude image combining is used, the two methods will be different due to the presence of additive noise; however, they are nearly identical at high SNR by Parseval's theorem.

The individual component ghost images, weighted by complex PSF values $h_k(x,y)$, may be combined either coherently or non-coherently (2). In this context, coherent image combining refers to the complex weighted sum which preserves phase, while non-coherent image combining refers to the (positive real) weighted sum of magnitudes or root sum of weighted squared magnitudes. For applications such as phase contrast that require phase sensitive detection it is essential to combine images coherently in order to preserve the phase. Likewise, in order to perform partial-Fourier acquisition such as partial-NEX, it is necessary to perform the homodyne reconstruction prior to magnitude detection. In this case, coherent image combining is desirable to gain improved estimate of background phase prior to homodyne detection.

Coherent image combining often uses matched filtering to maximize the SNR. In this case the image combining coefficients are based on the PSF which is assumed known or may be reasonably estimated. Define the spatially aligned separated ghost images by the vector **w**:

$$\begin{aligned} \mathbf{w} &= \begin{bmatrix} h_0(x,y) f(x,y) \\ \vdots \\ h_{N_g}(x,y) f(x,y) \end{bmatrix} = \begin{bmatrix} h_0(x,y) \\ \vdots \\ h_{N_g}(x,y) \end{bmatrix} f(x,y) \\ &= \mathbf{h}\, f(x,y) \end{aligned} \tag{6}$$

with vector **h** defined by eqn (6). The coherent combined image may be calculated as a weighted sum using the conjugate of the PSF estimates:

$$\begin{aligned} I(x,\ y) &= \hat{\mathbf{h}}(x,\ y)^{\mathrm{H}} \cdot \hat{\mathbf{w}}(x,\ y) \\ &= \hat{\mathbf{h}}(x,\ y)^{\mathrm{H}}\left[\mathbf{h}(x,\ y)\, f(x,\ y) + \tilde{\mathbf{n}}(x,\ y)\right] \end{aligned} \tag{7}$$

Where $\tilde{\mathbf{n}}$ denotes the noise after unmixing and spatial alignment. The estimate of the image is weighted by the squared norm $\|\mathrm{h}\|^2 = \mathrm{h}^{\mathrm{H}} \cdot \mathrm{h}$, which in many cases is approximately constant. If instead, the matched filter coefficient vector is first normalized to have unity norm (i.e. $\mathbf{h}/\|\mathbf{h}\|$), then the resultant image is weighted by $\|\mathbf{h}\|$. Alternatively, in cases where **h** is unknown, the image magnitude may be estimated non-coherently as the square root of the sum of the squares:

$$I(x,\ y) = \sqrt{\hat{\mathbf{w}}(x,\ y)^{\mathrm{H}} \cdot \hat{\mathbf{w}}(x,\ y)} \tag{8}$$

The matched filter coefficients may be estimated from the images themselves. In situations where multiple images are acquired, smoothing may be employed to reduce the error due to noise. For this case, one method which estimates the normalized coefficients (within a constant phase offset), is to form the time averaged sample covariance matrix for each pixel,

$$\mathbf{R}(x,\ y) = \sum_{t} \hat{\mathbf{w}}(x,\ y,\ t)\hat{\mathbf{w}}^{\mathrm{H}}(x,\ y,\ t) \tag{9}$$

where the variable *t* represents a time index, and averaging is performed over a number of frames during which $\mathbf{h}(x,y,t)$ has small time variation. An estimate of $\mathbf{h}(x,y)/\|\mathbf{h}(x,y)\|$ may be obtained by using the dominant eigenvector of **R**(x,y) (i.e. eigenvector with maximum eigenvalue) normalized by the root-sum-of-squares. The relative phase between components is preserved. For phase sensitive reconstruction, the same matched filter coefficients must be applied to the reference and desired images.

The inverse solution [eqn (4)] amplifies the noise causing a loss in signal-to-noise ratio (SNR) which is spatially varying. The loss in SNR relative to the artifact free image is calculated as (2,3)

$$SNR_{loss} \frac{1}{\sqrt{\left(\mathbf{S}^{\mathrm{H}}\mathbf{R}_n^{-1}\mathbf{S}\right)^{-1}_{(1,1)}\left(\mathbf{S}^{\mathrm{H}}\mathbf{R}_n^{-1}\mathbf{S}\right)_{(1,1)}}} \tag{10}$$

where the subscript (1,1) denotes the index of the matrix (first diagonal element) and the sensitivity matrix, **S**, is defined over the full FOV. The spatially varying denominator of eqn (10) is also referred to as the *g*-factor. Estimates of the g-factor were calculated from the sensitivities, **S**, and noise statistics, $\mathbf{R}_{\mathrm{n}}$, used in computing the unmixing matrix, **U**.

In the formulation above, all pixels are subject to phased array ghost elimination, and therefore suffer the SNR penalty [eqn (10)] due to ill-conditioning of the inverse solution, regardless of the actual number of ghosts cancelled at that pixel. The SNR losses for pixels with fewer actual ghosts may be greatly reduced by unmixing only the actual ghosts (22). This may be realized using a scheme that adaptively detects the number and position of ghosts for each pixel and applying the unmixing matrix for each pixel computed using a reduced rank sensitivity matrix with non-zero values corresponding to actual ghosts.

The PAGE solution [eqn (4)] has been shown (2,3,6) to optimize the signal-to-noise ratio (SNR). In the case of Cartesian sampling, this formulation may be recognized as a generalized form of the SENSE method (3) for reduced FOV imaging, which is a special case. In the case of accelerated imaging using SENSE, the alias ghosts are caused by the *k*-space sampling function (intentional undersampling), whereas in this formulation the distortion arises from continuous amplitude or phase errors, including space variant distortion. Phased array combining which optimizes SNR subject to nulling constraints is also known as the generalized sidelobe canceller (6). Phased array combining for optimized SNR without nulling constraints

has been shown (1) to provide a degree of artifact suppression for aliasing when the ghost spacing D is large relative to the effective width of the individual coil sensitivity profile (such as in a linear array). However, without nulling constraints, phased array combining optimized strictly for SNR provides very little ghost suppression for the general case where coils have significant overlap in field sensitivity and ghosts are more closely spaced.

Application to ghost artifacts in EPI

Ghost artifacts result from periodic phase and amplitude errors between lines of k-space (echoes). In applications such as echo-planar imaging (EPI), widely used for ultrafast imaging, examples of errors that cause ghost artifacts include EPI phase or delay misalignment and phase errors due to motion or flow. In general, ghost artifacts are a spatial variant distortion since the values depend on local effects such as flow or off-resonance due to chemical shift or susceptibility variation. A number of techniques (8-16) are used to minimize distortion and ghost artifacts. The phased array processing method for ghost cancellation adds yet another tool, which may be incorporated to further mitigate EPI distortion and artifacts.

Application to multi-shot EPI with both interleaved and sequential, non-interleaved phase encode acquisition order is considered for cardiac imaging. In applications such as in cardiac imaging where the T_2* value is relatively short, images are typically acquired using multiple shots with relatively short echo-trains. To avoid ghost artifacts, images are frequently acquired using an interleaved phase encode order (9,10), although interleaved phase encode order has several drawbacks. Drawbacks of this approach are the geometric and intensity distortion caused by off-resonance phase errors due to chemical shift or susceptibility variation (8), distortion due to in-plane flow, increased echo train length which results when echo shifting is employed, and distortion due to echo delay misalignment. Using a sequential, non-interleaved phase encode order with an echo train length, ETL, will cause N_g=ETL−1 ghosts spaced D=FOV/ETL, and therefore has not been considered viable. A non-interleaved phase encode acquisition order has benefits if the ghosts may be eliminated. Cancellation of ghosts by means of phased array processing makes non-interleaved strategies possible. In this case, the drawbacks cited above for interleaved acquisition are traded for widely spaced ghosts, which in turn are cancelled by phased array processing. The distortion due to off-resonance is illustrated in Fig. 3 for both interleaved and sequential phase encode order for ETL=4. In Fig. 3, the raw signal phase vs phase encode line (k_y) and real PSF are plotted for interleaved, interleaved with echo-time shifting, and sequential phase encode orders. Echo time shifting mitigates the gross degradation to the PSF but has a slight shift of the peak which corresponds to geometric distortion. The sequential order causes ghosting which may be mitigated by the parallel imaging approach to provide a single undistorted PSF peak. A comparison of these two strategies is illustrated in Fig. 4 which uses images from an oil/water phantom. In the conventional image reconstruction using interleaved phase encode order (upper image) there is a geometric distortion in the phase encode (vertical) direction which causes a spatial shift of pixels containing oil (inner cylinder) relative to pixels containing water (outer cylinder). The oil cylinder is shifted downward closer to the water. Using the PAGE method with sequential phase encode order, the reduction of geometric distortion is evident since the oil and water cyclinders appear concentric with more equal spacing.

In the case of sequential, non-interleaved acquisition, pixels with an off-resonance frequency of Δf lead to a periodic k-space (phase) weighting, with period ETL Δk_y, where Δk_y is the spacing between phase encode lines. The complex k-space weights (ignoring a constant phase factor), due to off-resonance at a pixel (x,y), are $H_m(x,y)=e^{j[m\Delta\varphi]}$, where $\Delta\varphi=2\pi\Delta f(x,y)\Delta TE$, where ΔTE is the echo spacing, and m=0, … , ETL−1 is an integer index corresponding to $k_y=m\Delta k_y$ repeating with period ETL Δk_y. The corresponding values of the discrete point spread

function $h_m(x,y)$ (space variant) are derived from the $(N_g + 1)$-point discrete Fourier transform, i.e. $h_m(x,y)=\mathrm{DFT}[H_m(x,y)]$.

The PSF values, h_k, for fat and water will be different, and a degree of fat suppression is achieved by simply using the h_0 weighted signal (assumed to be on resonance) and ignoring the other components, h_m ($m > 0$) (2,17). Separation of fat and water images using a two-echo SSFP sequence was demonstrated by setting the echo spacing ΔTE for 180° phase rotation for the chemical shift due to fat (18). A simple off-resonance correction was calculated using the coefficients H_m which correspond to the water ± fat images. This may be further generalized using a multi-point Dixon fat–water separation method with additional echoes (arbitrary echo spacing) and iterative least square solution as described by Reeder *et al.* (19).

B1-maps estimates and auto-calibration

The surface coil field maps (B1-maps), $s_i(x,y)$, required for determining the phased array combiner coefficients (unmixing matrix), **U** [defined by eqn (4)], may be estimated from ghost-free images; this is true for either scheme (Fig. 1 or 2). Ghost-free images suitable for calculating sensitivity maps may be acquired prior to the imaging scan. Alternatively, ghost-free images may be acquired from the imaging data in an auto-calibrating manner, depending on the application. In the application of PAGE to eliminating ghosts which arise due to transient approach to interrupted steady-state SSFP imaging, B1-maps were simply estimated from images for the later cardiac phases which were ghost-free (2). In the case of EPI imaging, a time-varying phase encode order may be employed which temporally modulates each ghost image to a different temporal frequency, thereby enabling the individual ghosts to be separated (17). In this scheme, diagrammed in Fig. 5 for the case of ETL=4, the phase encode order in each multi-echo shot is varied such that after N=ETL time frames a full set of raw k-space data has been acquired at each echo time TE. A lower temporal resolution ghost free image suitable for estimating the complex coil sensitivities may be derived by integration or filtering in a manner similar to the TSENSE method (23). Each of the superimposed ghosts is at a different temporal frequency and may be separated. The image weighted by the PSF value h_0 is calculated by simple integration of an integer multiple of ETL frames or equivalently filtering. The kth ghost at temporal frequency k/N (normalized by frame rate) is weighted by h_k and may be calculated either by FFT or by frequency translation followed by integration (i.e. summation of the pixel time series after multiplication by a time varying exponential to shift the temporal frequency component to 0 frequency). The separated ghost images may then be spatially aligned. A weighted sum may be used for calculating the B1-map in order to optimize the SNR. It may be recognized that this scheme of temporal variation of phase encode order for full-FOV acquisitions permits a generalization of the UNFOLD method formulated for reduced FOV accelerated imaging (20).

The ghost-free images are then used to calculate the complex sensitivity used for computing the inverse solution using steps that may include normalization, spatial smoothing and optional thresholding for voxel exclusion. In this case, ghost-free images were normalized by the RSS magnitude to obtain raw complex sensitivities with image modulus removed. A sample correlation matrix for each pixel (x,y) is calculated from raw complex sensitivities, and then a small degree of spatial smoothing (a 3 × 3 pixel spatial lowpass kernel) is applied to reduce the noise. The sample correlation removes the image phase while preserving the relative phase between coils which is essential to coherent phased array combining. The estimate of the relative complex coil sensitivities is derived from the smoothed correlation values by calculating the dominant eigenvector of the sample correlation matrix for each pixel, i.e. the eigenvector is proportional to $[s_1(x,y), \ldots s_{N_c}(x,y)]^{\mathrm{T}}$, which is used to compose the matrix **S** defined by eqn (2).

Experimental parameters

The PAGE method was applied to multi-shot EPI cardiac functional imaging using a trueFISP (SSFP) readout. Experiments were conducted using a 1.5 T Siemens Sonata MR imaging system. A custom eight-element cardiac phased array (Nova Medical Inc., Wilmington, MA, USA) was used, consisting of two four-element linear arrays (24 × 6 cm element size with long dimension oriented along the S/I direction and without gap in the L/R direction), with one array positioned on the chest, and the second array positioned on the back of the subject. Raw data including prescan noise was acquired for all scans and images were reconstructed off-line using Matlab (The Mathworks, Natick, MA, USA).

Breath-held cine imaging of a single short axis slice was performed using an ECG-triggered, segmented acquisition of *k*-space over a number of heartbeats. A sequential (i.e. non-interleaved) phase encode order was used which results in periodic ghosts using a conventional recontruction without parallel imaging. A multi-echo SSFP imaging sequence was used with the following parameters: ETL=3, bandwidth 1.5 kHz/pixel, echo times TE=1.5, 2.6, 3.7 ms, TR=5.1 ms, 50° RF flip angle and 8 mm slice thickness. Data were collected over approximately 75% of the cardiac cycle.

Results are shown for a study performed on a normal healthy volunteer, performed under a protocol approved by the Institutional Review Board of the National Heart, Lung and Blood Institute. The FOV was 320 × 240 mm with an image matrix of 192 × 144, with corresponding in-plane spatial resolution approximately 1.7 × 1.7 mm^2. The 144 phase encodes were acquired using 12 views-per-segment (cardiac phase) during a breath-hold period of 12 heartbeats. This resulted in a temporal resolution of 4 × TR=20.4 ms. The surface coil field maps (B1-maps) were derived from an average across the cardiac cycle.

RESULTS

Short axis images of the heart are shown in Fig. 6 for a single cardiac phase during mid-diastole. Ghost artifacts that arise using a sequential phase encode order with echo-train length ETL=3 are evident in Fig. 6(a) which combines individual coil images using the-root-sum-of-squares method without using phased array ghost elimination. The phase encode direction is top–bottom in these figures. The phased array (PAGE) separated component magnitude images, desired image plus 1/3, and 2/3 FOV ghosts, weighted by $h_0(x,y)$, $h_1(x,y)$ and $h_2(x,y)$, are shown in Fig. 6(b)-(d), respectively, with the same grayscale (window and level) used for all images. The image of Fig. 6(e) is the root-sum-of-squares combination of Fig. 6(b)-(d). Figure 6(f)-(h) shows the magnitude of the three images with phased array ghost elimination by an alternative method shown in Fig. 2, weighted by $H_0(x,y)$, $H_1(x,y)$ and $H_2(x,y)$, respectively. These images correspond to acquisition at separate echo-times TE_1, TE_2 and TE_3, respectively. The complex images at these echo times may be used to calculate separate fat and water images (19). The root-sum-of-squares combination of Fig. 6(f)-(h) is shown in Fig. 6(i).

The h_0 weighted image of Fig. 6(b) is primarily due to the on-resonance water component. It is possible to simply use the magnitude image of Fig. 6(b), which will provide a slight fat suppression and slight increase in SNR (particularly in low SNR regions), assuming a reasonable field homogeneity (shim). The SNR improvement results from dropping the noise-only ghost components which reduces the noise bias resulting from magnitude detection. In comparison, the 'fat suppressed' h_0 weighted image calculated shown in Fig. 6(b) is equivalent to the sum of H_0, H_1, and H_2 weighted complex images ($h_0=H_0 + H_1 + H_2$) calculated using the alternative method which applies SENSE to the images reconstructed from deinterleaved *k*-space lines. The root-sum-of-squares combined magnitude images of Fig. 6(e) and (i) are almost identical for high SNR pixels. The ghost artifacts due to both off resonance and in-plane flow are effectively removed by means of this phased array processing technique. Furthermore,

using a sequential acquisition, the repetition time *TR* is reduced significantly by eliminating echo-shifting.

A high degree of ghost artifact elimination is achieved. This artifact is suppressed to the noise level or below. PAGE causes a reduction in SNR by the SENSE *g*-factor. In this example using eight coils and rate 3, the *g*-factor measured in the heart region had mean value 1.2 and 95% of pixels in the region had values <1.5.

CONCLUSION

We have presented a general methodology for application of parallel imaging to elimination of periodic ghosts, referred to as phased array ghost elimination. This method is capable of eliminating ghosting due to spatial variant distortion mechanisms such as local off-resonance or flow, and had broad application including widely used EPI imaging. The PAGE method for ghost cancellation may result in greater flexibility in designing acquisition strategies.

Acknowledgment

The authors would like to thank Dan Herzka and Vinay Pai for their development of multi-echo FISP sequences.

Contract/grant sponsors: Intramural Research Program of the NIH; National Heart, Lung and Blood Institute.

Abbreviations used

ETL, echo train length; PAGE, phased array ghost elimination; PSF, point spread function; SENSE, sensitivity encoding; SSFP, steady-state free precession.

REFERENCES

1. Roemer PB, Edelstein WA, Hayes CE, Souza SP, Mueller OM. The NMR phased array. Magn. Reson. Med 1990;16:192–225. [PubMed: 2266841]
2. Kellman P, McVeigh ER. Ghost artifact cancellation using phased array processing. Magn. Reson. Med 2001;46(2):335–343. [PubMed: 11477638]
3. Pruessmann KP, Weiger M, Scheidegger MB, Boesiger P. SENSE: sensitivity encoding for fast MRI. Magn. Reson. Med 1999;42:952–962. [PubMed: 10542355]
4. Kuhara, S.; Kassai, Y.; Ishihara, Y.; Yui, M.; Hamamura, Y.; Sugimoto, H. A novel EPI reconstruction technique using multiple RF coil sensitivity maps; Proc. 8th Scientific Meeting International Society of Magnetic Resonance Medicine; 2000. p. 154
5. Griswold MA, Jakob PM, Edelman RR, Sodickson DK. Alternative EPI acquisition strategies using SMASH. Proc. Int. Soc. Magn. Reson. Med 1998:423.
6. Johnson, DH.; Dudgeon, DE. Array Signal Processing: Concepts and Techniques. Prentice-Hall; Englewood Cliffs, NJ: 1993. p. 355-371.
7. Walsh DO, Gmitro AF, Marcellin MW. Adaptive reconstruction of phased array MR imagery. Magn. Reson. Med 2000;43:682–690. [PubMed: 10800033]
8. Farzaneh F, Riederer SJ, Pelc NJ. Analysis of T_2 limitations and off-resonance effects on spatial resolution and artifacts in echo-planar imaging. Magn. Reson. Med 1990;14:123–139. [PubMed: 2352469]
9. McKinnon GC. Ultrafast interleaved gradient-echo-planar imaging on a standard scanner. Magn. Reson. Med 1993;30:609–616. [PubMed: 8259061]
10. Feinberg DA, Oshio K. Phase errors in multi-shot echo planar imaging. Magn. Reson. Med 1994;32:535–539. [PubMed: 7997122]
11. Wan X, Gullberg GT, Parker DL, Zeng GL. Reduction of geometric and intensity distortions in echo-planar imaging using a multireference scan. Magn. Reson. Med 1997;37:932–942. [PubMed: 9178246]

12. Wan X, Parker DL, Lee JN, Buswell HR, Gullberg GT. Reduction of phase error ghosting artifacts in thin slice fast spin-echo imaging. Magn. Reson. Med 1995;34:632–638. [PubMed: 8524034]
13. Wetter DR, McKinnon GC, Debatin JF, von Schulthess GK. Cardiac echo-planar MR imaging: comparison of single- and multiple-shot techniques. Radiology 1995;194:765–770. [PubMed: 7862976]
14. Reeder SB, Atalar E, Bolster BD Jr, McVeigh ER. Quantification and reduction of ghosting artifacts in interleaved echo-planar imaging. Magn. Reson. Med 1997;38:429–439. [PubMed: 9339445]
15. Reeder SB, Atalar E, Faranesh AZ, McVeigh ER. Multi-echo segmented *k*-space imaging: an optimized hybrid sequence for ultrafastcardiac imaging. Magn. Reson. Med 1999;4:375–385. [PubMed: 10080287]
16. Epstein FH, Wolff SD, Arai AE. Segmented *k*-space fast cardiac imaging using an echo-train readout. Magn. Reson. Med 1999;41:609–613. [PubMed: 10204886]
17. Herzka DA, Kellman P, Aletras AH, Guttman MA, McVeigh ER. Multi-shot EPI-SSFP in the heart. Magn. Reson. Med 2002;47(4):655–664. [PubMed: 11948726]
18. Flask, CA.; Lewin, JS.; Duerk, JL. Lipid elimination with an echo-shifting N/2-ghost acquisition; Proc. 12th Annual Meeting of ISMRM; Kyoto. May, 2004; p. 269
19. Reeder SB, Wen Z, Yu H, Pineda AR, Gold GE, Markl M, Norbert J, Pelc NJ. Multicoil Dixon chemical species separation with an iterative least-squares estimation method. Magn. Reson. Med 2004;51(1):35–45. [PubMed: 14705043]
20. Madore B, Glover GH, Pelc NJ. Unaliasing by Fourier encoding the overlaps using the temporal dimension (UNFOLD), applied to cardiac imaging and fMRI. Magn. Reson. Med 1999;42:813–828. [PubMed: 10542340]
21. Kellman P, Guttman MA, Herzka DA, McVeigh ER. Phased array ghost elimination (PAGE) for segmented SSFP imaging with interrupted steady-state. Magn. Reson. Med 2002;48(6):1076–1080. [PubMed: 12465121]
22. Larkman, DJ.; Callaghan, MF.; Hajnal, JV. Optimising artifact removal in PPI corrected GRASE imaging; Proc. 11th Annual Meeting of ISMRM; Toronto. July, 2003; p. 1062
23. Kellman P, Epstein FH, McVeigh ER. Adaptive sensitivity encoding incorporating temporal filtering (TSENSE). Magn. Reson. Med 2001;45(5):846–852. [PubMed: 11323811]

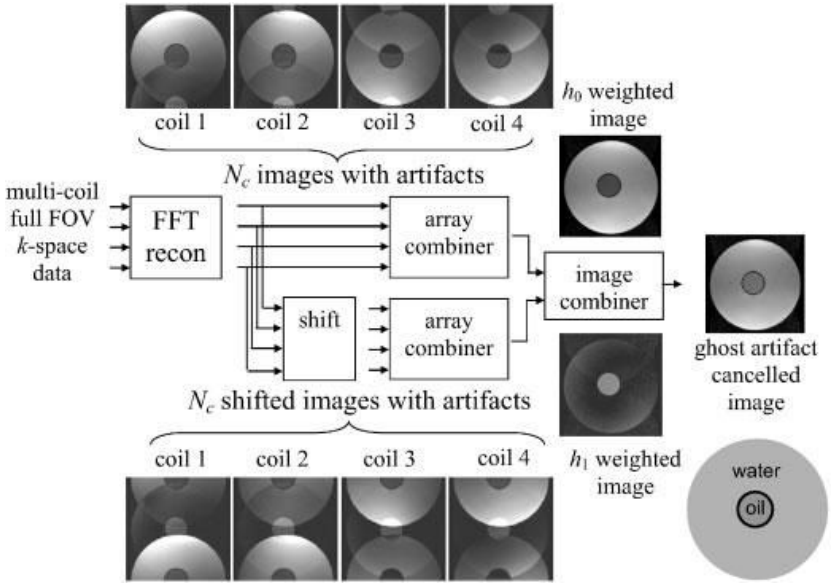

Figure 1.
Block diagram of PAGE method applied directly to full FOV images with ghosts (illustration images for N_c=4 coils and N_g=1 ghost artifact with D=FOV/2)

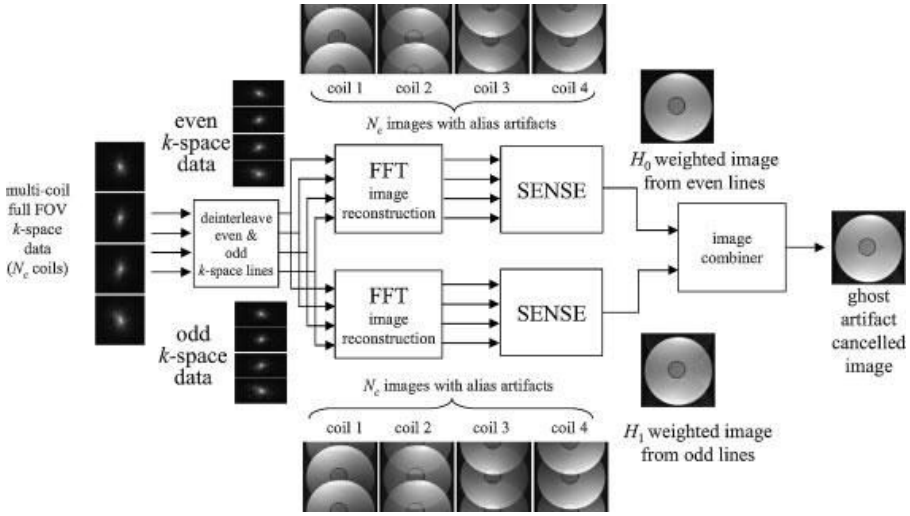

Figure 2.

Block diagram of PAGE method using alternative implementation applying SENSE reconstruction directly to deinterleaved *k*-space data (illustration images for N_c=4 coils and N_g=1 ghost artifact with D=FOV/2)

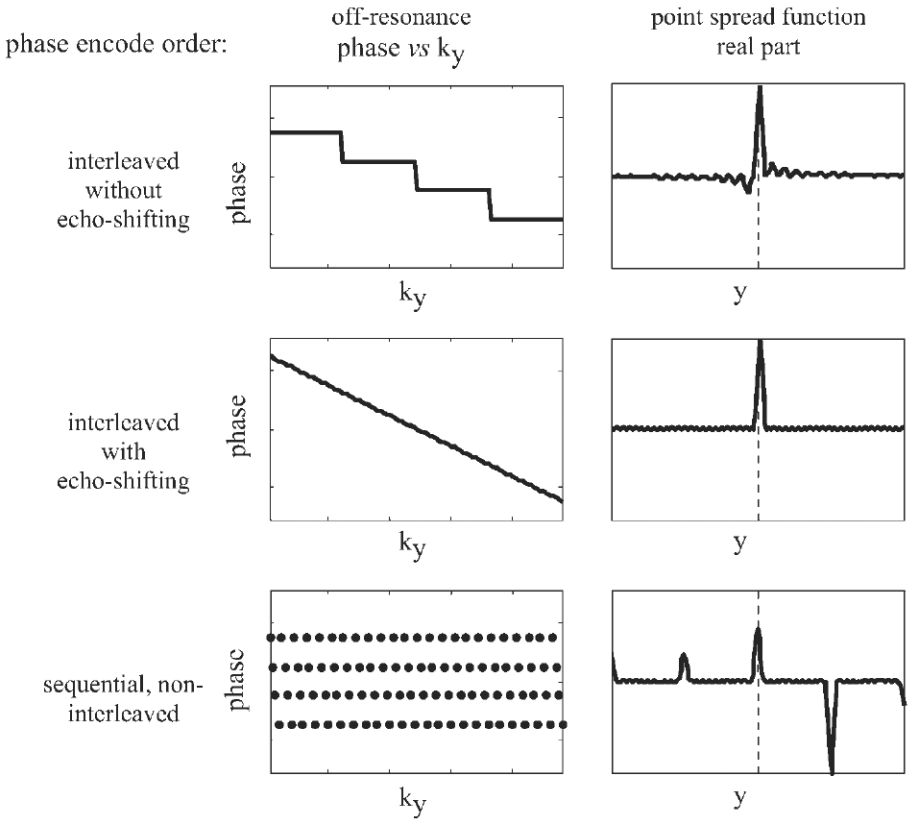

Figure 3.
Illustration of multi-shot EPI distortion due to off-resonance phase for various phase encode orders showing distortion of point spread function using interleaving without echo time shifting (top row), geometric distortion (shift) using interleaving with echo time shifting (middle row), and periodic ghosting using sequential phase encode order (bottom row)

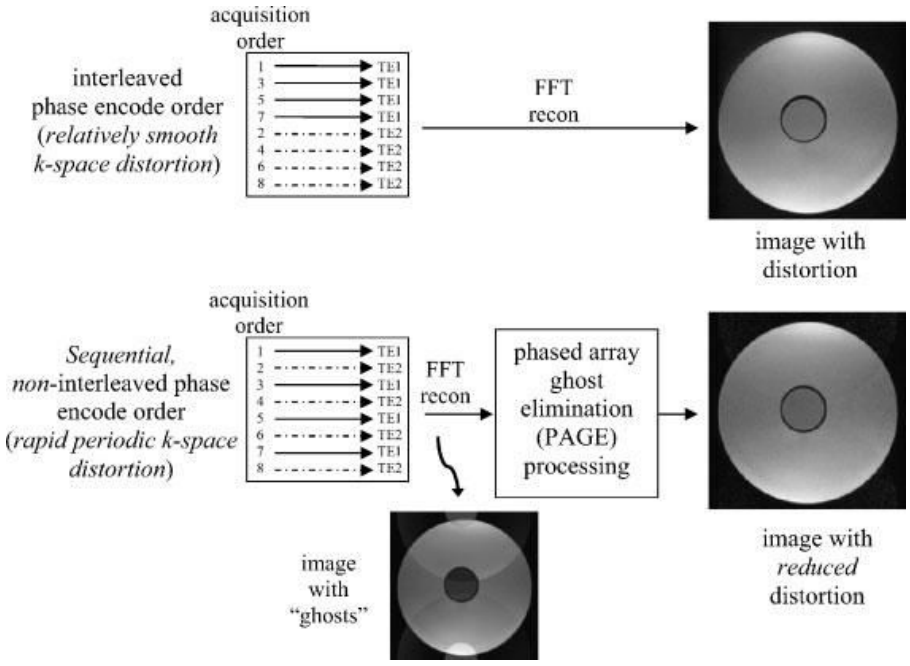

Figure 4.
Comparison of strategies for multi-shot EPI imaging with and without PAGE, illustrated using oil (inner cylinder) and water (outer cylinder) phantom images, with ETL=2. Note the reduction of geometric distortion using PAGE

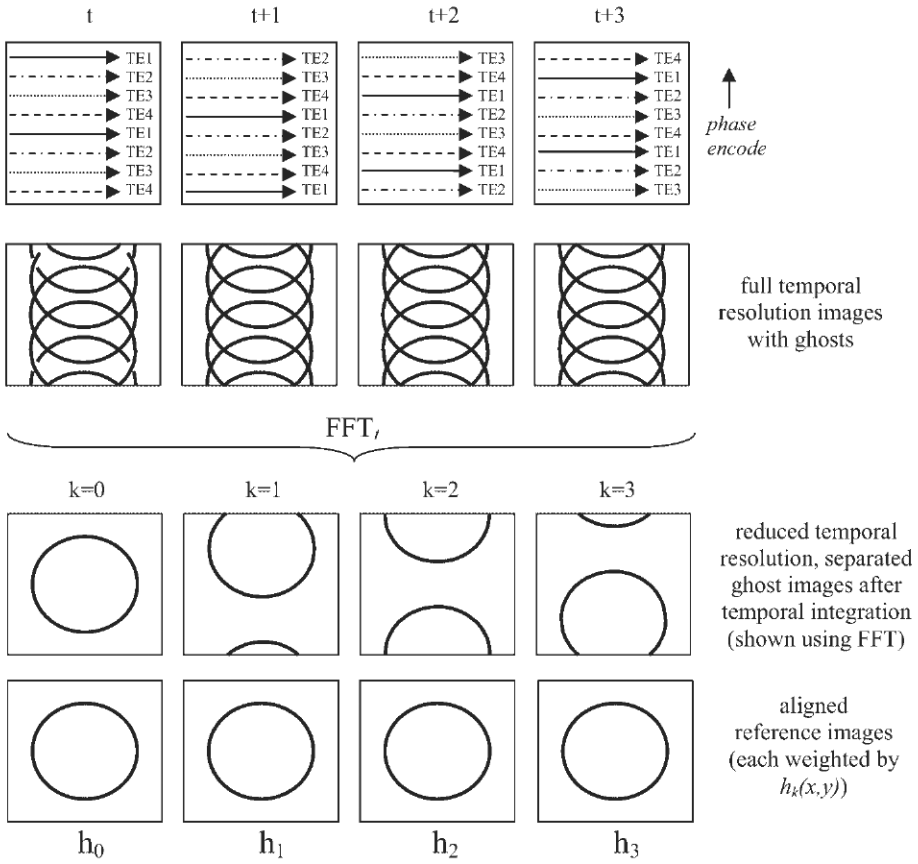

Figure 5.

Auto-calibration scheme for EPI which produces lower temporal resolution ghost free reference images for calculating coil sensitivity profiles. The phase encode order is temporally varied such that all lines of *k*-space are acquired at each echo time after *N*=ETL frames. The separated ghost images are each weighted by their corresponding point spread function values $h_k(x,y)$

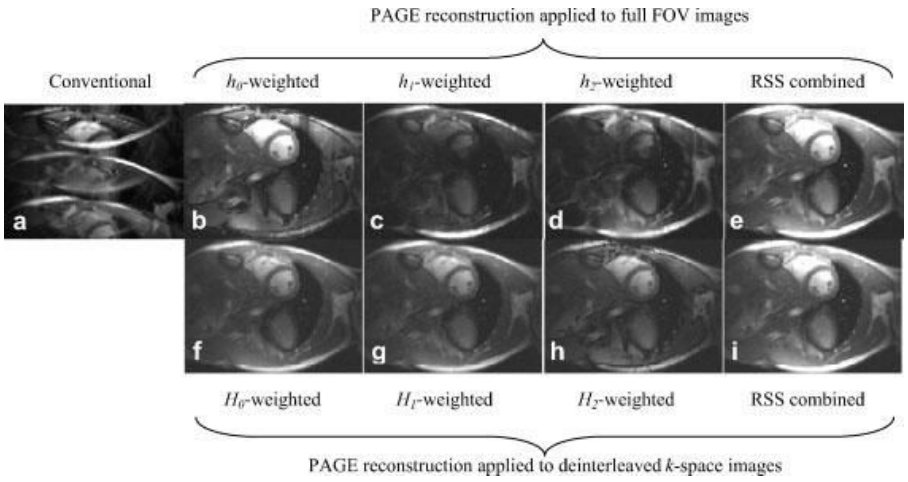

Figure 6.

Images comparing conventional image reconstruction with ghosts (left column) and PAGE reconstructed images (right columns) for ECG triggering segmented multi-echo trueFISP cine acquisition. The top row shows PAGE reconstruction applied to the full FOV image, with individual separated ghost image components (h_i weighted) shown in columns 2–4, and the ghost cancelled RSS combined magnitude images shown in right column. The bottom row shows PAGE reconstruction applied to the deinterleaved *k*-space images, with separate images for each echo time (*TE*) (H_i weighted) shown in columns 2–4, and the ghost cancelled RSS combined magnitude images shown in right column